2-22-2023

Boron Nitride Nanotubes: Force Field Parameterization, Epoxy Interactions, and Comparison with Carbon Nanotubes for High-Performance Composite Materials

Swapnil S. Bamane
Michigan Technological University

Michael B. Jakubinek
National Research Council Canada

Krishan Kanhaiya
University of Colorado Boulder

Behnam Ashrafi
National Research Council Canada

Hendrik Heinz
University of Colorado Boulder

See next page for additional authors

Recommended Citation

Bamane, S., Jakubinek, M., Kanhaiya, K., Ashrafi, B., Heinz, H., & Odegard, G. (2023). Boron Nitride Nanotubes: Force Field Parameterization, Epoxy Interactions, and Comparison with Carbon Nanotubes for High-Performance Composite Materials. *ACS Applied Nano Materials, 6*(5), 3513-3524. http://doi.org/10.1021/acsanm.2c05285

Retrieved from: https://digitalcommons.mtu.edu/michigantech-p/16987

Follow this and additional works at: https://digitalcommons.mtu.edu/michigantech-p

 Part of the Mechanical Engineering Commons

ACS APPLIED NANO MATERIALS

www.acsanm.org

Article

Boron Nitride Nanotubes: Force Field Parameterization, Epoxy Interactions, and Comparison with Carbon Nanotubes for High-Performance Composite Materials

Swapnil S. Bamane, Michael B. Jakubinek, Krishan Kanhaiya, Behnam Ashrafi, Hendrik Heinz, and Gregory M. Odegard*

Cite This: *ACS Appl. Nano Mater.* 2023, 6, 3513−3524

Read Online

ACCESS | Metrics & More | Article Recommendations | Supporting Information

ABSTRACT: Boron nitride nanotubes (BNNTs) are a very promising reinforcement for future high-performance composites because of their excellent thermo-mechanical properties. To take full advantage of BNNTs in composite materials, it is necessary to have a comprehensive understanding of the wetting characteristics of various high-performance resins. Molecular dynamics (MD) simulations provide an accurate and efficient approach to establish the contact angle values of engineering polymers on reinforcement surfaces, which offers a measure for the interaction between the polymer and reinforcement. In this research, MD simulations and experiments are used to determine the wettability of various epoxy systems on BNNT surfaces. The reactive interface force field (IFF-R) is parameterized and utilized in the simulations to accurately describe the interaction of the epoxy monomers with the BNNT surface. The effect of the epoxy monomer type, hardener type, local atomic charges, and temperature on the contact angle is established. The results show that contact angles decrease with increases in temperature for all the epoxy/hardener systems. The bisphenol-A-based epoxy system demonstrates better wettability with the BNNT surface than the bisphenol-F based epoxy system. Furthermore, the MD predictions demonstrate that these observations are validated with experimental results, wherein the same contact angle trends are observed for macroscopic epoxy drops on nonwoven nanotube papers. As wetting properties drive the resin infusion in the reinforcement materials, these results are important for the future manufacturing of high-quality BNNT/epoxy nanocomposites for high-performance applications such as aerospace and aeronautical vehicles.

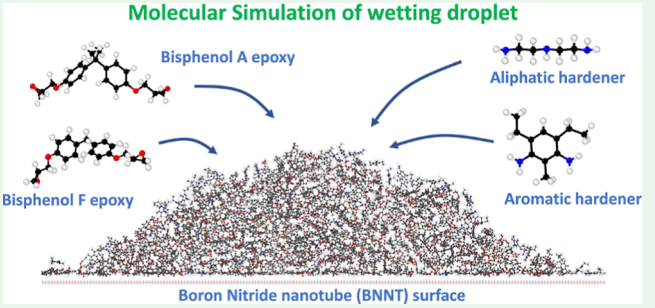

KEYWORDS: *contact angle, surface tension, processibility, composite materials, aerospace materials, molecular dynamics*

1. INTRODUCTION

Polymer matrix composites (PMCs) are currently being considered as a primary structural material for aerospace vehicles. Reinforced nanocomposite materials have been shown to provide exceptional material properties over traditional PMCs.[1−3] Boron nitride nanotubes (BNNTs) exhibit remarkable mechanical properties at higher temperatures, electrical insulation, and radiation shielding[4−10] and have recently been shown to be an excellent reinforcement in nanocomposite materials.[4,11−14] However, to fabricate high-performance BNNT-reinforced PMCs efficiently and effectively, a thorough understanding of the BNNT/polymer interfacial interaction is needed.[15,16]

Resin-reinforcement wettability is a key design parameter in the manufacture of high-quality PMCs. Wettability is often quantified by determining the contact angle of liquid droplets on reinforcement surfaces. Molecular dynamics (MD) simulations can be used to analyze the resin/reinforcement interaction at interfaces, predict the corresponding contact angle, and provide physical insight into the observed interfacial behavior.[2,3,17−22] MD simulations are often easier to control and faster in comparison to laboratory experiments. Although MD-predicted material properties may not always agree perfectly with experimental measurements, MD predictions offer direct physical insight into nano-scale atomic interactions at the interface. MD has been used to study the wetting properties of water and polymer resins on graphite and metallic surfaces.[23−31] Recently, Bamane et al.[32] used MD simulations to study the wettability of high-performance polymer systems on aromatic carbon surfaces to determine the relative levels of processibility of carbon nanotube composites. Thus far, the

Received: December 8, 2022
Accepted: February 13, 2023
Published: February 22, 2023

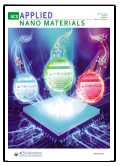

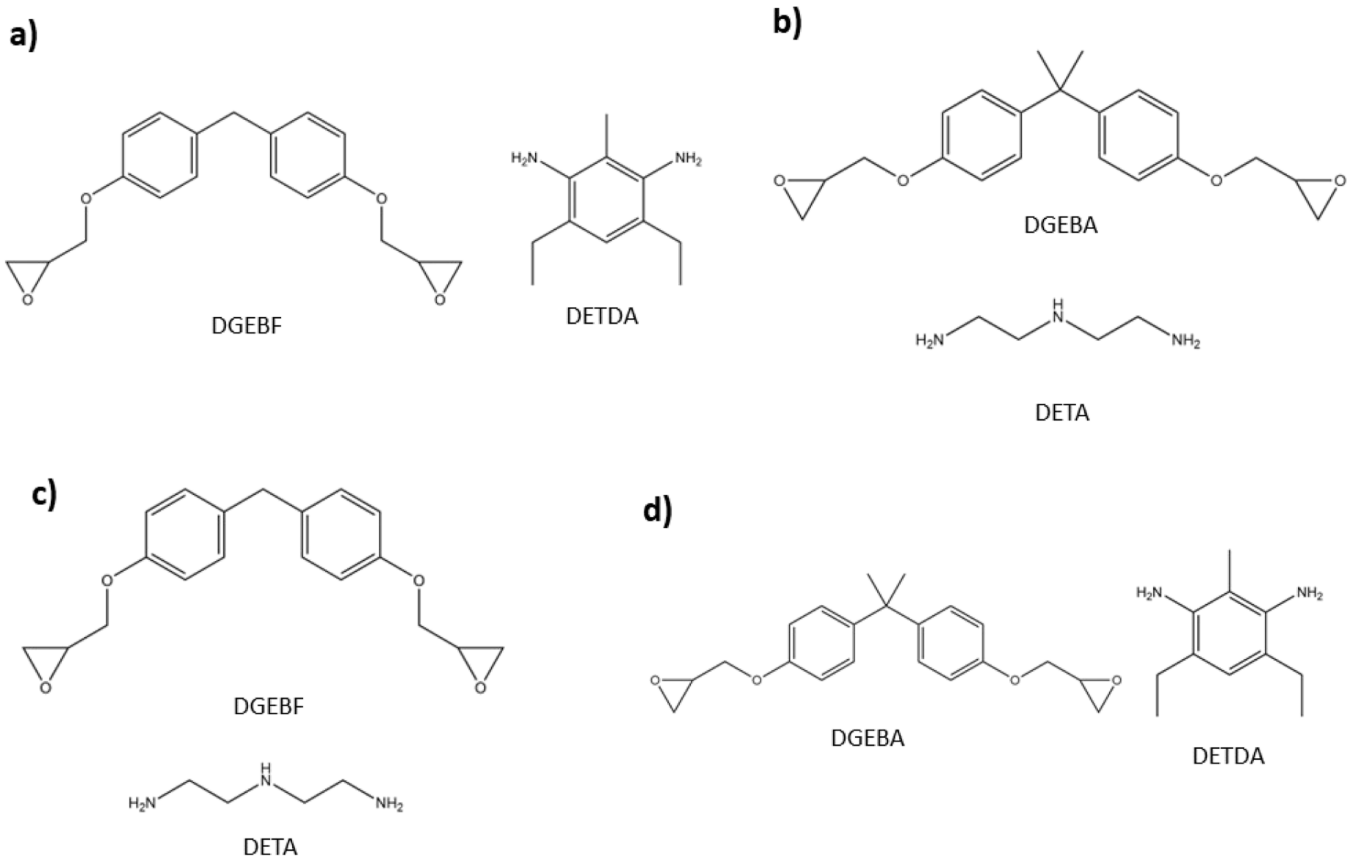

Figure 1. Molecular structures of epoxy systems: (a) bisphenol-F epoxy with an aromatic hardener, (b) bisphenol-A epoxy with an aliphatic hardener, (c) bisphenol-F epoxy with an aliphatic hardener, (d) bisphenol-A epoxy with an aromatic hardener.

wetting properties of polymer resin systems on BNNT surfaces have not been studied extensively. Therefore, to take full advantage of the excellent properties of BNNTs in nanocomposites and establish the most compatible resins with BNNTs, MD-based procedures to predict the wettability of various resin systems on BNNT surfaces need to be developed and validated through comparison with experiments.

There has been recent interest in using the reactive interface force field (IFF-R) developed by Heinz et al.[33,34] to model high-performance polymer systems and PMCs.[21,35,36] IFF-R has proven its ability to accurately predict the thermomechanical properties of various polymer materials.[21,35,36] IFF-R is especially accurate for simulating interfacial interactions between the matrix and reinforcement materials with its ability to assign accurate partial charges on molecules.[37] However, IFF-R has not yet been parameterized to model BNNT surfaces and the virtual π electrons to capture internal polarity effects. To efficiently perform wetting simulations using MD, it is necessary to parameterize IFF-R for BNNT surfaces.

The objective of this study is to provide insight into the epoxy/BNNT wetting process with the help of experimental observations and MD simulations. First, IFF-R is parametrized for BNNT surfaces. Second, the parametrized IFF-R is used in MD simulations to predict the contact angle values of four epoxy systems on BNNT surfaces as a function of temperature. Physical insight into the corresponding results is quantified by interaction energy (IE) calculations of the epoxy functional groups. Carbon nanotubes (CNTs) have been the focus of many wetting studies,[17,18,38] hence the wetting properties of epoxy with CNTs and BNNTs are compared. Furthermore, model validation experiments are performed by measuring the contact angle values of the same epoxy systems on macroscale BNNT and CNT buckypaper surfaces.

2. MATERIALS

The four epoxy-based polymer systems analyzed in this study are listed below, and Figure 1 shows their molecular structures. These systems were chosen because of their engineering relevance, ease of processing, and relatively low viscosity.

- Bisphenol-F epoxy with an aromatic hardener: diglycidyl ether bisphenol F (DGEBF) epoxy monomer and a diethyltoluenediamine (DETDA) hardening agent. The stoichiometric molar ratio of resin to hardener is 2:1. This system is commercially marketed as EPON 862/EPIKURE W.
- Bisphenol-A epoxy with an aliphatic hardener: diglycidyl ether bisphenol A (DGEBA) epoxy monomer and a diethylenetriamine (DETA) hardening agent. The stoichiometric molar ratio of resin to hardener is 5:2. This system is commercially marketed as EPON 828/EPIKURE 3223.
- Bisphenol-F epoxy with an aliphatic hardener: DGEBF epoxy monomer and a DETA hardening agent. The stoichiometric molar ratio of resin to hardener is 5:2.
- Bisphenol-A epoxy with an aromatic hardener: DGEBA epoxy monomer and a DETDA hardening agent. The stoichiometric molar ratio of resin to hardener is 2:1.

3. MOLECULAR MODELING PROCEDURES

Molecular modeling and simulations were performed using the Large-Scale Atomic/Molecular Massively Parallel Simulator (LAMMPS) software package developed by Scandia National

https://doi.org/10.1021/acsanm.2c05285
ACS Appl. Nano Mater. 2023, 6, 3513−3524

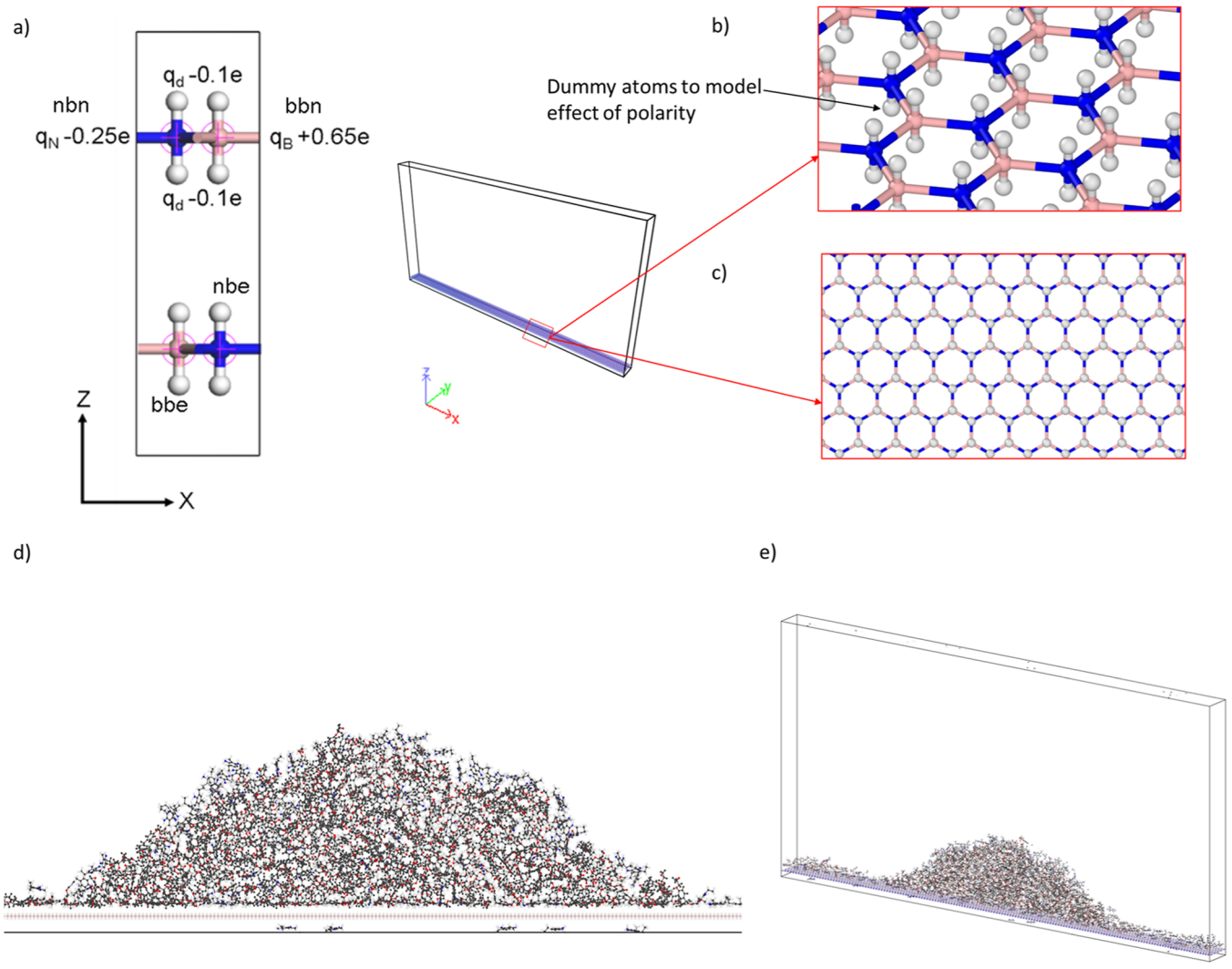

Figure 2. Molecular model of the BNNT surface with (a) the unit cell of BNNT, (b) dummy atoms representing virtual π electrons, and (c) the BNNT surface view in the *XY* plane (d) snapshot at 2 ns simulation time of contact angle simulation in the *XZ* plane (e) snapshot at 2 ns of the contact angle simulation in 3D.

Laboratories.[39,40] This section describes the parameterization for hexagonal boron nitride (h-BN) in IFF-R and the molecular modeling of the BNNT surfaces and resin droplets with MD. Details on the contact angle calculation method and IE analysis are also included. IFF-R parameters were used to model the epoxy polymer systems.[33] The geometric mixing rule was applied to define the pair coefficients between interatomic interactions. It is important to note that other powerful potentials could also be implemented in a study such as this.[41]

3.1. Parameterization of h-BN. Figure 2 shows the molecular structure of h-BN with three boron atoms and three nitrogen atoms forming six-membered rings. Each boron atom and nitrogen atom are connected to three nitrogen and three boron atoms, respectively, to generate an infinite graphene-like sheet. The structure of h-BN is isoelectronic with graphene, with added polarity between more electropositive boron atoms and more electronegative nitrogen atoms along the covalent B−N bonds. Accordingly, the parameterization is analogous to previous efforts to validate IFF-R[33] parameters for graphene, graphite, and aromatic molecules that include virtual π electrons for accurate interfacial property predictions.[42−44] In this work, IFF-R for h-BN utilizes the energy expression of the fixed-bond polymer consistent force field, which includes a 9-6 Lennard-Jones potential,[33] and a Morse potential for nonlinear bonded interactions.

The h-BN model was refined relative to graphite by adding the internal dipole moments of the B−N bonds via atomic charges, matching crystal lattice parameters, and tuning the force constants such that the covalent bond vibrations correlated well with the experimental Raman spectrum.[8] The charges on the boron and nitrogen atoms were estimated from NMR data,[45] expectations from the extended Born model,[37] and measured dipole moments of similar compounds. Accordingly, boron carries a charge of +0.45 ± 0.05*e*, and nitrogen carries an equal and opposite charge of −0.45 ± 0.05*e*.[45−47] Force field parameters associated with the bonding between virtual electrons and boron or nitrogen atoms, virtual electron charge, bond angle bending, and Lennard-Jones interactions were adopted from graphite parameters.[42] As graphite and h-BN are isoelectronic, the virtual electrons were treated in the same manner by including two virtual electron clouds per atom with a mass of 1 g/mol each that was subtracted from the boron and nitrogen masses, as shown in

https://doi.org/10.1021/acsanm.2c05285
ACS Appl. Nano Mater. 2023, 6, 3513−3524

Table S1 in the Supporting Information. The development of the force field parameters for boron, nitrogen, and the virtual electron atoms is detailed in the Supporting Information.

3.2. BNNT Surface. A pseudo two-dimensional setup for contact angle simulations with MD (Figure 2) has been shown to be efficient and accurate.[23,24,30] Bamane et al.[32] predicted the contact angle values of several high-performance polymers on aromatic carbon surfaces as a function of temperature. A similar approach was used herein to predict contact angles for the epoxy resins on flat BNNT surfaces. A periodic simulation box of size ~400 Å × 21 Å × 205 Å was used to create the monolayer BNNT surface as shown in Figure 2. Figure 2 also shows the dummy atoms modeled to represent the virtual electrons to capture the effect of multipole moments. Detailed discussions on virtual electrons can be found elsewhere.[48] The initial atomic coordinates were generated using the "Lattice" command in LAMMPS. The total number of atoms in the surface model was 9600, which included 1600 boron atoms, 1600 nitrogen atoms, and 2 virtual π electrons per boron and nitrogen atoms.

3.3. CNT Surface. The monolayer CNT surface MD model had a periodic simulation box size of ~400 Å × 21 Å × 210 Å, as shown in the Supporting Information (Figure S1). The initial atomic positions were generated using the "Lattice" command in the LAMMPS software package. The total number of atoms in the surface model was 9720, which included 3240 C atoms and 2 dummy atoms per C atom.

3.4. Wetting Simulations. Similar to Bamane et al.,[32] the wetting simulation procedure consisted of two steps: the monomer droplet formation and the monomer-surface contact simulations. Figure S2 shows a graphical representation of the MD workflow. More information about the development of the framework in terms of simulation time, polymer chain length effect, and model size can be found elsewhere.[32] Both droplet formation and contact angle simulations were performed for five replicate models for each resin system to account for the statistical variation in the predictions of contact angle values. The wetting simulations were performed at elevated temperatures ranging from 87 to 177 °C.[32]

To create the droplet models in Step I, resin monomers were added to empty simulation boxes using the initial equilibrium configurations of the monomers. ChemDraw[49] was used to efficiently obtain the initial equilibrated monomer structures. After importing into LAMMPS, a more comprehensive energy minimization was performed using the conjugate-gradient method in LAMMPS. The droplet formation simulations were performed in the constant volume and temperature (*NVT*) ensemble with a timestep size of 1 fs. Table S5 shows the number of atoms modeled in the droplet model per resin system.

In Step II, the monomer droplet models were inserted in the BNNT surface simulation boxes. The initial position of the droplets in the contact simulations was kept less than 7 Å away from the top of the BNNT surface so that there would be van der Waals interactions between the BNNT surface and the monomer droplet. MD simulations were performed for 2 ns in the *NVT* ensemble with a timestep size of 1 fs. Some of the contact simulations at higher temperatures of 147 and 177 °C required a timestep size of 0.1 fs to fully capture the high velocity of the atoms. Figure 2 shows a snapshot of the contact angle simulation at 2 ns for bisphenol F epoxy with the aliphatic hardener system at 87 °C.

3.5. Contact Angle and IE Calculations. The previously established method of calculating the contact angle values from the MD simulation data by Bamane et al.[32] was used. Specifically, an array of two-dimensional 1 Å × 1 Å windows was created in the $x-z$ plane of the simulation box, and the mass density of each window was determined. The corresponding mass density map data generated at the end of the contact simulations was analyzed using an in-house Python script. A graphical representation of the contact angle values was created using an RStudio script. Further details about this procedure can be found elsewhere.[32]

The IE between individual chemical groups in the droplets and the surface was calculated using the "compute group/group" command in LAMMPS. The long-range coulombic interactions were included by using pair style "lj/cut/coul/long". A global cutoff radius of 10 Å was used to calculate the Coulombic interactions. Long-range forces were calculated using the particle−particle particle-mesh solver defined by the "kspace" command with style "pppm" in LAMMPS. The IE was determined using

$$\mathrm{IE}_{1,2} = E(1,2) - (E_1 + E_2) \quad (1)$$

where $\mathrm{IE}_{1,2}$ is the IE between atoms in group 1 and group 2; E_1 is the energy of atoms present in group 1; E_2 is the energy of atoms present in group 2; and $E(1,2)$ is the total energy of atoms present in groups 1 and 2. The IE was calculated by assigning the surface atoms to group 1 and the monomer molecules to group 2. The IE values were averaged over the last 200 ps of the contact simulations. It is important to note that higher magnitudes of IE in the negative direction correspond to stronger interactions.

4. EXPERIMENTAL PROCEDURES

Nanotube papers, commonly called buckypaper, were produced by dispersion of nanotube powders in methanol, followed by vacuum filtration and drying to yield paper-like nonwoven sheets. The BNNTs were small-diameter, few-walled BNNTs (BNNT-P by Tekna, Canada). These BNNTs are produced using an h-BN feedstock and purified to remove some impurities, in particular elemental boron, as reported in detail elsewhere.[50,51] Transmission electron microscopy of BNNTs produced in this process shows high-quality BNNTs with typical diameters of 5 nm and, most commonly, 2−5 walls.[50] For a CNT comparison, thin (d_{avg} ~ 10 nm), multi-walled CNTs (*NC7000* by NANOCYL, Belgium) were employed. Two epoxy systems were used in the experiments, namely EPON 828 with EPIKURE 3223 and EPON 862 with EPIKURE W (Miller-Stephenson). The epoxy systems were mixed, based on the ratios employed in the modeling work, using a planetary mixer (Thinky ARE-310) at 2000 rpm with 30 s of mixing and 30 s of defoaming. Conversions from the stoichiometric ratios used in modeling to the weight ratios required experimentally are shown in the Supporting Information (Tables S3 and S4). The resulting mixing ratios were:

- 28.54 parts hardeners per 100 parts resin for EPON 862/EPIKURE W, which is slightly higher than the manufacturer-recommended mix ratio (26.4:100), and
- 12.1 parts hardener per 100 parts resin for EPON 828/EPIKURE 3223, which is nearly equal to the manufacturer-recommended ratio (12:100).

Following mixing, small drops (5−10 μL, as measured by fitting images of the initial drop shape to the Young−Laplace equation) were placed on buckypaper samples, and their contact angles were measured using a contact angle optical tensiometer (Attension Theta by Biolin Scientific, Sweden) with a temperature-controlled stage. The measured contact angle values decreased over time and typically approached stable values within 1 min, as shown in the

https://doi.org/10.1021/acsanm.2c05285
ACS Appl. Nano Mater. 2023, 6, 3513−3524

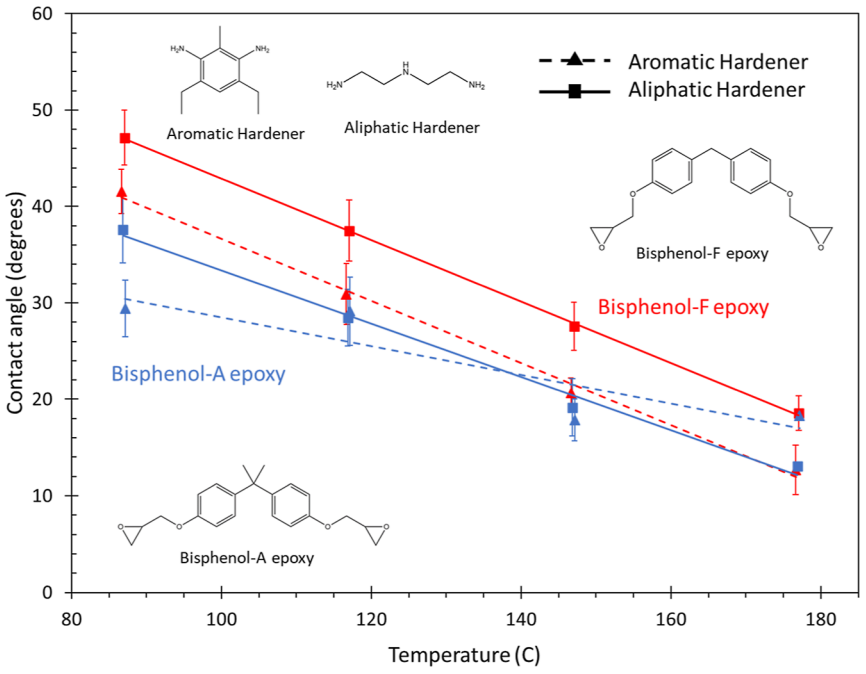

Figure 3. Contact angle vs temperature for all epoxy systems predicted by MD simulations. Lines represent the curve fits to the data, and error bars represent the standard error of the predictions.

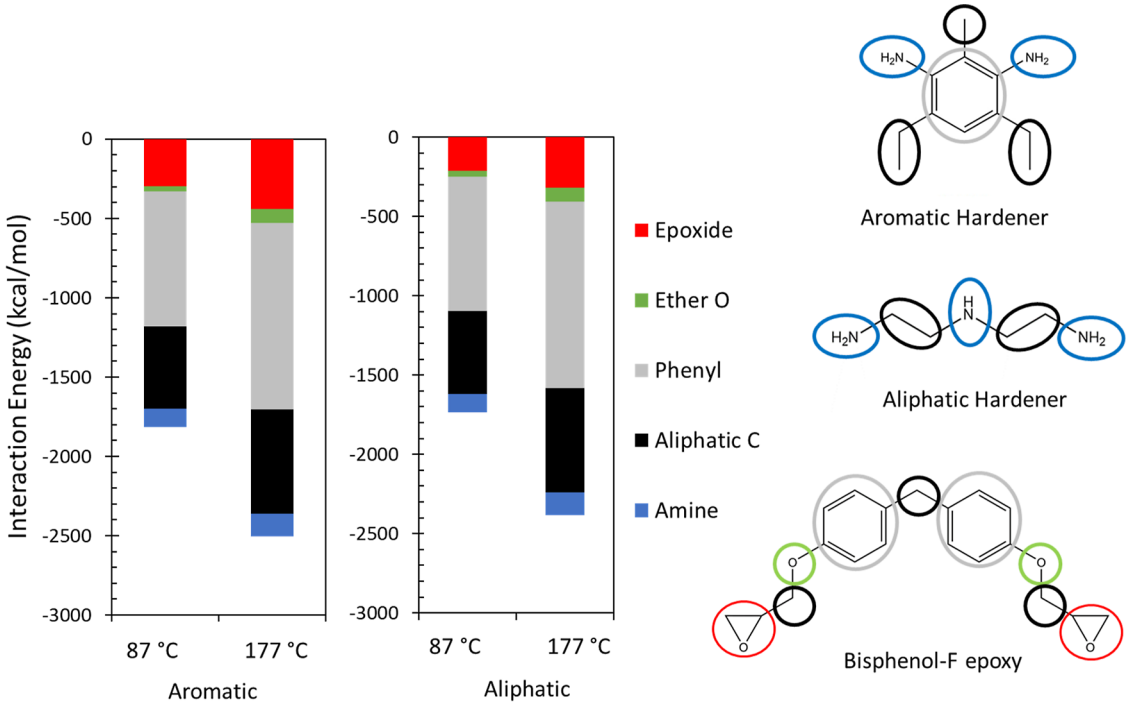

Figure 4. Comparison of the distribution of IE by functional groups in the bisphenol-F epoxy systems at 87 and 177 °C. The average standard error of IE values of the entire system (not shown in the figure) is 52 kcal/mol.

Supporting Information (Figures S5–S8). The final contact angles were calculated by averaging the dynamic contact angle values over 56 to 60 s of test time for each test.

Measurements were performed in a sequence alternating from CNT paper to BNNT paper and back to CNT paper. Agreement between the angles measured on the CNT paper before and after the measurements on the BNNT paper verified that the comparison between nanotube types was not affected by changes in the cure state of the epoxy during the time of the experiment. A minimum of three droplets were measured for each set of conditions.

Nanocomposite samples were also prepared by wetting buckypaper samples with the bisphenol-F epoxy mixed with an aromatic hardener. This epoxy infusion was performed by placing a small amount of the resin onto a buckypaper sample on a hotplate at 90 °C. The sample, which was supported on a release film, was tilted to help spread the resin fully across the buckypaper and then allowed to sit for 10 min before gently dabbing the surface with a lint-free wipe to remove excess resin. The wetted buckypaper was then vacuum-bagged on a hotplate at 100 °C to support full infusion and remove remaining excess resin and cured at 120 °C for 2 h while maintaining the

https://doi.org/10.1021/acsanm.2c05285
ACS Appl. Nano Mater. 2023, 6, 3513−3524

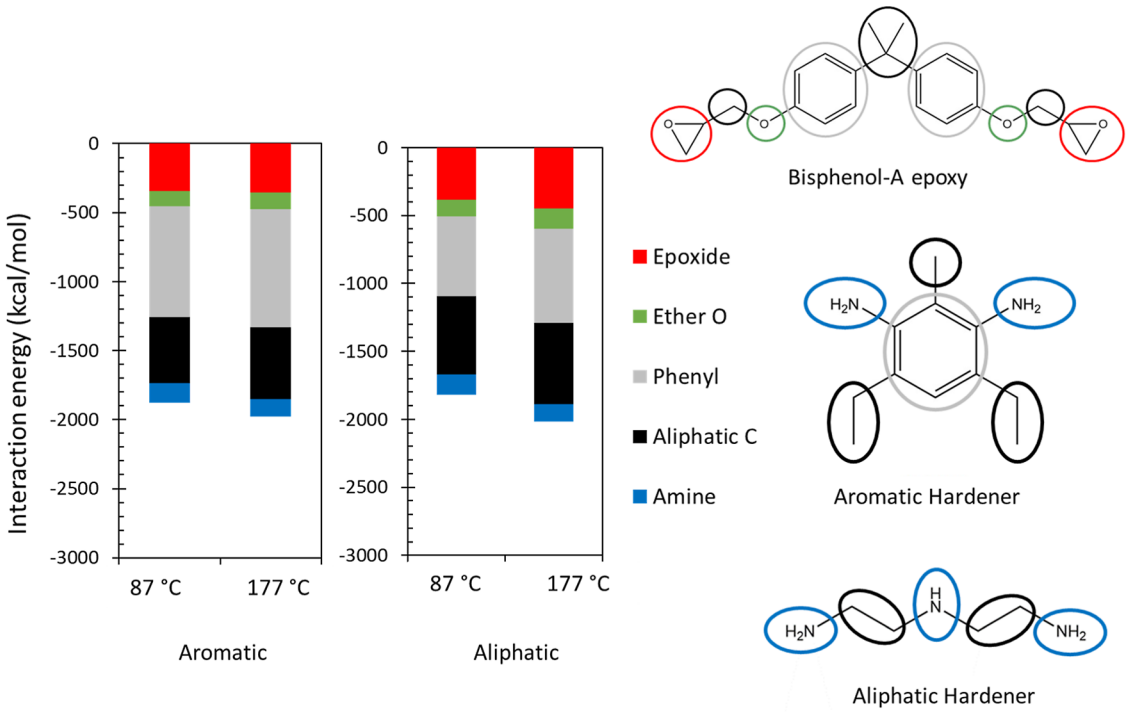

Figure 5. Comparison of IE distribution by functional groups for bisphenol-A epoxy systems at 87 and 177 °C. The average standard error of IE values of the entire system (not shown in the figure) is 61 kcal/mol.

vacuum. Figure S3 shows the process of wetting the BNNT buckypaper and the BNNT/epoxy infusion process. CNT/epoxy buckypaper samples were prepared following the same procedure. The comparison of properties of CNT and BNNT composites prepared by this infusion process is discussed in the Supporting Information (Section S4).

5. RESULTS AND DISCUSSION

Figure 3 shows the comparison between the contact angle values of the bisphenol-F epoxy systems predicted by MD simulations. It can be clearly observed that the contact angle values decrease linearly with increases in temperature. This trend is expected as increases in temperature enable further mobility (kinetic energy) of the epoxy monomers on the surface, thus allowing them to more easily achieve lower-energy configurations within the droplet and at the interface, thus driving down the contact angle. The contact angle values for the bisphenol-F epoxy with the aromatic hardener are consistently lower than those with the aliphatic hardener. The difference in the contact angle values is consistent throughout the temperature range and is observed to be nearly 6°. It is clear that the bisphenol-F epoxy with the aromatic hardener shows better wettability than the aliphatic hardener system on the BNNT surface.

The contact angle values for the bisphenol-A-based epoxy systems are shown in Figure 3. The contact angle values for both systems decrease with increases in temperature. It is clear that the contact angle values of the bisphenol-A epoxy with the aromatic hardener are lower than those with the aliphatic hardener at lower temperatures. At 117 and 147 °C, there is no statistical difference between the contact angle values between the two systems. At 177 °C, the contact angle values for the aliphatic hardener system are lower than those of the aromatic hardener system.

The distribution of IE values for each functional group in both bisphenol-F epoxy systems is shown in Figure 4. The IE contributed by the phenyl rings in the aromatic hardener system is 333 ± 1 kcal/mol greater than that of the aliphatic hardener system at 87 °C and 240 ± 1 kcal/mol greater at 177 °C. Because of the lower resin-to-hardener ratio for the aromatic system, there is a smaller number of large epoxy monomers in the aromatic system. This allows greater mobility of monomers on the surface, including the aromatic hardener groups. Increases in the IE contributed by the epoxide groups in the aliphatic hardener system are because of the higher ratio of epoxy to hardener monomers relative to the aromatic system. As shown in Figure 4, the overall effect of differences in phenyl- and epoxide-group IE values results in lower contact angle values for the aromatic system.

The contributed IE of the different chemical groups in the two bisphenol-A systems with the BNNT surface is shown in Figure 5. The IE distribution is compared between the two systems at 87 and 177 °C temperatures to provide insight into the change in the wettability trend around 130 °C. For the aromatic hardener system, the interaction between the droplet and the surface is primarily driven by phenyl groups. When the temperature is increased from 87 to 177 °C, there is an increase in the IE contributed by the phenyl rings by 54 ± 1 kcal/mol, which accounts for 44% of the total increase in IE, whereas aliphatic carbon groups contribute to 32%. However, in the aliphatic hardener system, the increase in IE with increasing temperature is dominated by both phenyl and epoxide groups. The increase in IE contributed by the phenyl rings is 103 ± 1 kcal/mol, which is 52% of the total increase in IE; and the epoxide group interaction is increased by 66 ± 1 kcal/mol, which is 33% of the total increase in IE. This demonstrates that at the higher temperature, the influence of the epoxide groups drives the wettability of the aliphatic hardener system. This influence of the epoxide groups is not

https://doi.org/10.1021/acsanm.2c05285
ACS Appl. Nano Mater. 2023, 6, 3513−3524

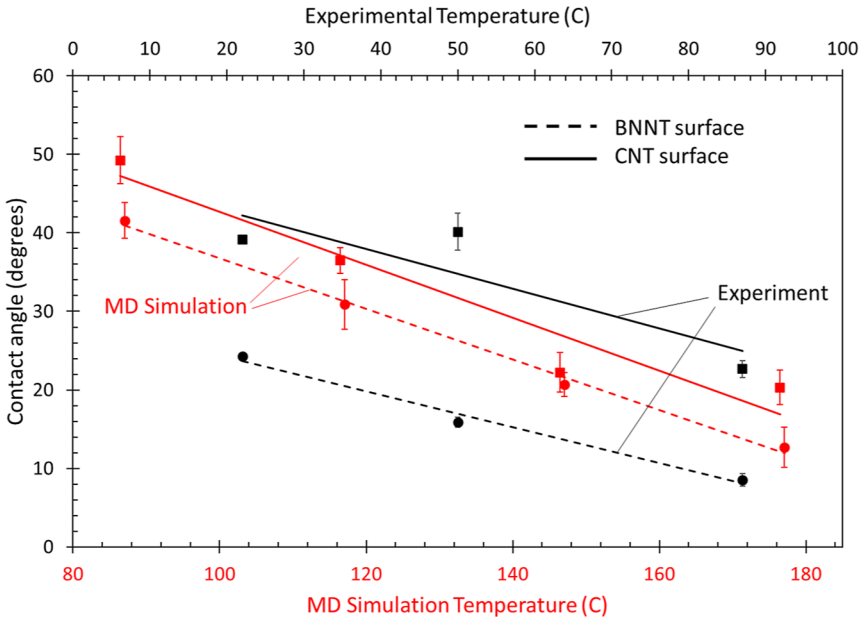

Figure 6. Comparison of experimental and MD-predicted contact angle values as a function of temperature for the bisphenol-F epoxy with the aromatic hardener.

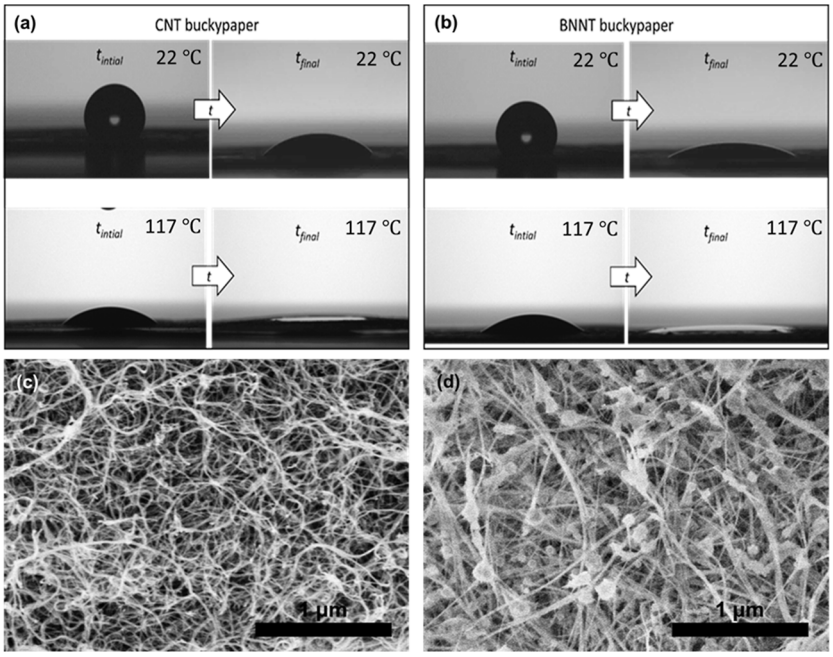

Figure 7. Contact angle observations of bisphenol-F epoxy with an aromatic hardener at 22 and 117 °C on (a) CNT buckypaper and (b) BNNT buckypaper. SEM images of the buckypaper surfaces for (c) CNT buckypaper and (d) BNNT buckypaper. Scale bars are 1 μm.

observed in the aromatic hardener system because of the preferential adsorption of phenyl rings on the BNNT surface, providing steric hindrance against epoxide group interactions. Figure S9 shows the orientation of phenyl rings with the BNNT surface. It is important to note that this study is only focused on non-cross-linked monomers, and the IE distribution of the functional groups of the cross-linked polymer system will likely be different than that shown in Figure 5. The prediction of the IE distribution for these epoxy systems will be a subject of future work.

From Figure 3, the bisphenol-A epoxy systems show better wettability than the bisphenol-F epoxy systems at 87, 117, and 147 °C. At 177 °C, the bisphenol-F system with the aromatic hardener shows better wettability than the bisphenol-A system with the aromatic hardener. From Figures 4 and 5, it is evident that the total IE is the highest for the bisphenol-F epoxy resin system with an aromatic hardener at 177 °C. This system shows the highest increase in IE contributed by phenyl rings (39%) when the temperature is increased from 87 to 177 °C. At 177 °C, the effect of increased interactions of epoxide groups in the bisphenol-A epoxy systems is lower than the effect of increased interaction of phenyl groups in bisphenol-F epoxy with the aromatic hardener, hence exhibiting lower contact angle values.

https://doi.org/10.1021/acsanm.2c05285
ACS Appl. Nano Mater. 2023, 6, 3513−3524

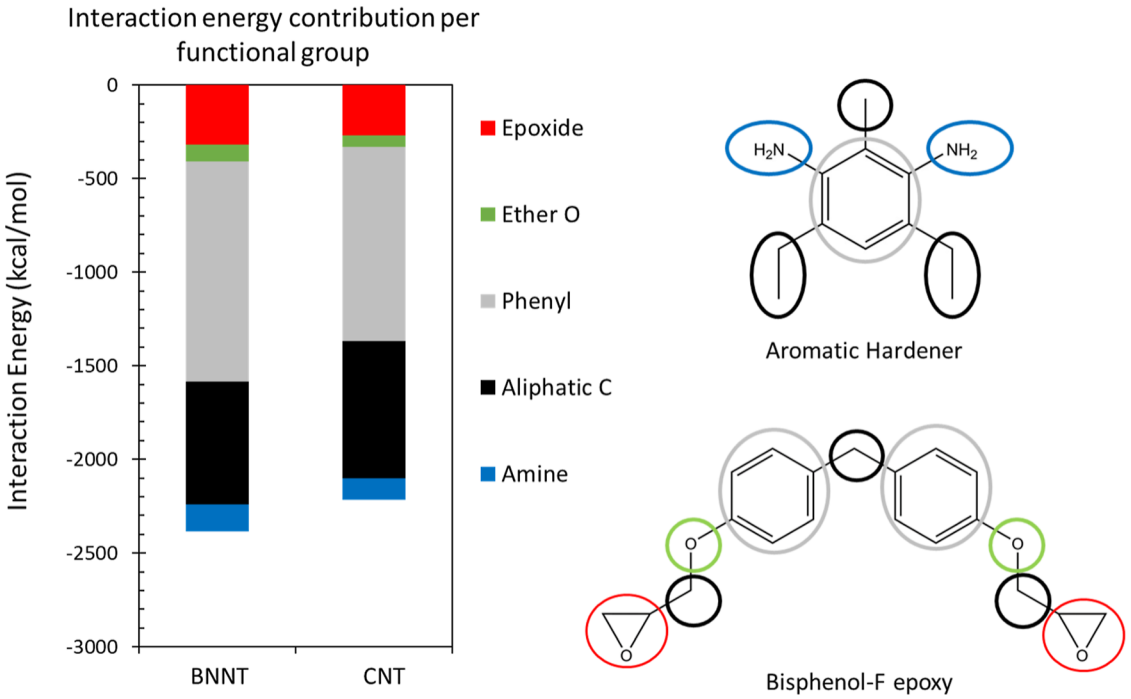

Figure 8. Comparison of IE distribution by functional groups for bisphenol-F epoxy with aromatic hardeners on BNNT and CNT surfaces at 177 °C. The average standard error of IE values of the entire system (not shown in the figure) is 56 kcal/mol.

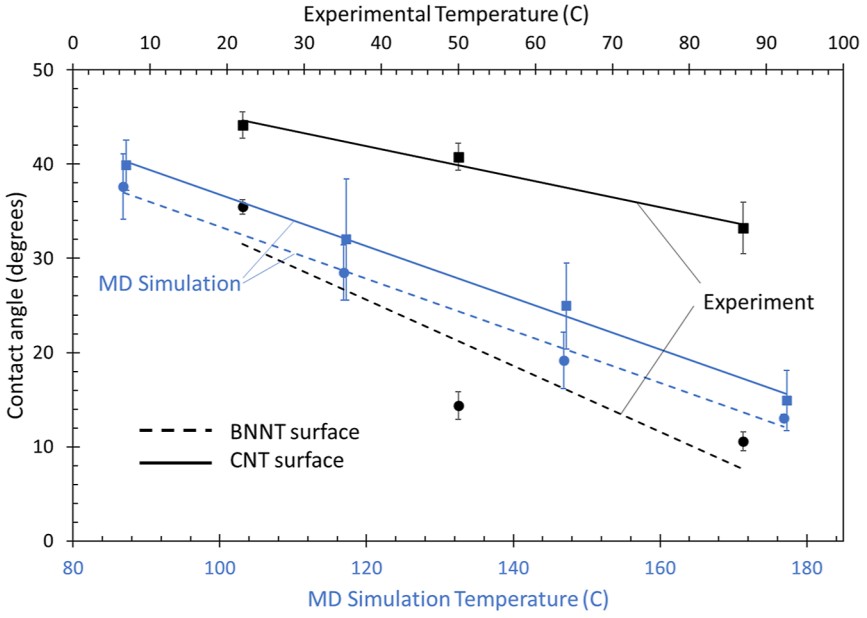

Figure 9. Comparison of experimental and MD predicted contact angle values as a function of temperature for the bisphenol-A epoxy with the aliphatic hardener.

The predicted and experimentally measured values of the contact angle on BNNT and CNT surfaces are plotted against temperature (two different scales) in Figure 6 for the bisphenol-F epoxy with the aromatic hardener. Wetting experiments are observable at the macro-scale, where a relatively large drop interacts with the surface of a nonwoven paper composed primarily of nanotubes, and MD simulations are carried out at the nano-scale, with a difference of about 9 orders of magnitude in the length scale. Therefore, a comparison of the absolute contact angle values between experiments and MD simulation is not direct, but a comparison of trends in wettability as a function of temperature is more directly comparable. Therefore, two different temperature ranges representing experimental data and MD simulation data are shown in Figure 6. Both experimental measurements and MD predictions show a decrease in contact angle values on both surfaces with increasing temperatures. The experimental and predicted data clearly show higher wettability of the bisphenol-F epoxy system on BNNT surfaces relative to CNT surfaces over the entire respective temperature ranges, except at 147 °C, where there is no statistical distinction between the predicted contact

https://doi.org/10.1021/acsanm.2c05285
ACS Appl. Nano Mater. 2023, 6, 3513−3524

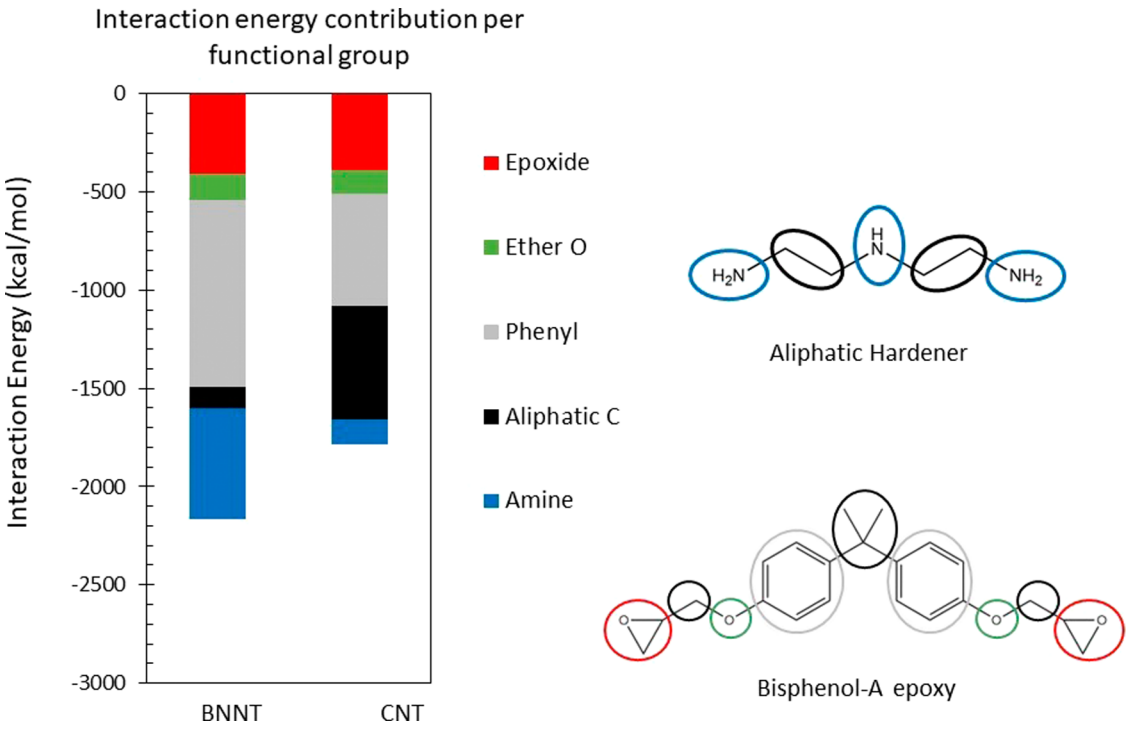

Figure 10. Comparison of IE distribution by functional groups for the bisphenol-A epoxy with aliphatic hardeners on BNNT and CNT surfaces at 147 °C. The average standard error of IE values of the entire system (not shown in the figure) is 61 kcal/mol.

angles. The measured values show a difference of ∼20° in the contact angle values for the two surfaces throughout the entire experimental temperature range of 22−87 °C.

Figure 7 shows a visual comparison of contact angle values for the CNT and BNNT surfaces observed in the experiments. The difference in the contact angles for the bisphenol-F epoxy system is clearly observed at room temperature, while the contact angles are low, showing excellent wetting for both nanotube paper types at 117 °C. Figure 7 also shows the SEM images of CNT and BNNT buckypaper surfaces used in these experiments.

Figure 8 shows the predicted IE values of the bisphenol-F epoxy system with the aromatic hardener on BNNT and CNT surfaces. It is evident that the epoxy interactions with both BNNT and CNT surfaces are dominated by phenyl groups. The IE contributed by phenyl rings with the BNNT surface is higher by 139 ± 1 kcal/mol than with the CNT surface. The IE contribution of aliphatic C groups on the BNNT surface is 28% of total IE, whereas on the CNT surface, it is 33%. This clearly shows that the aliphatic C groups show a better interaction with the CNT surface than with the BNNT surface. The epoxide groups show higher interaction with the BNNT surface by 50 ± 1 kcal/mol. This is due to the attraction between positively charged B atoms and negatively charged O atoms in the epoxide groups. The surrounding negatively charged N atoms cause the O atoms to further shift closer to the positively charged B atoms, resulting in stronger interactions between the surface and epoxide groups. The higher interactions of phenyl rings and epoxide groups with the BNNT surface appear to provide higher wettability relative to the CNT surface.

Figure 9 shows the predicted and experimentally measured contact angle values of the bisphenol-A epoxy system with aliphatic hardeners on BNNT and CNT surfaces. It is important to note that Figure 9 has different temperature scales corresponding to simulation and experimental measurement. Because nano- and micro-scale droplet contact angles are not expected to be the same, as discussed above, the linear fits shown in Figure 9 are not extrapolated. For both surfaces, the predicted and measured contact angle values decrease with increasing temperature. The predicted and measured average contact angles are lower for the BNNT surface throughout the temperature range (although not statistically different for the predictions). Comparable trends observed in Figures 6 and 9 between measured and predicted values validate the developed MD framework to simulate the wetting experiments. The improvement in the comparison of predicted and measured contact angles could be achieved with much larger MD models, which is not currently feasible given limited computational resources.

The functional group IE contributions for the BNNT and CNT surfaces for the bisphenol-A epoxy resin and aliphatic amine hardeners are shown in Figure 10. From the data in Figure 10, it is evident that the IE of the resin system is higher for BNNT surfaces, which supports the wettability trends in Figure 9. Similar to the bisphenol-F-based resin system, the resin interactions on the BNNT surface are dominated by the phenyl groups. The IE contributed by phenyl groups is 954 ± 1 kcal/mol, which is 44% of total IE, whereas the interactions on the CNT surface are jointly dominated by phenyl and aliphatic carbon groups. On the CNT surface, phenyl groups contribute 573 ± 1 kcal/mol, which is 32% of the total IE, and aliphatic carbon groups contribute 572 ± 1 kcal/mol, which is 32% of the total IE. Amine groups present in the aliphatic hardener show stronger interactions on the BNNT surface than on the CNT surface. This is due to the attraction between negatively charged N atoms in the amine groups and positively charged B atoms. This indicates that the hardener molecules have a significant impact on the wetting of the bisphenol-A system on the BNNT surface. The relatively high interactions

https://doi.org/10.1021/acsanm.2c05285
ACS Appl. Nano Mater. 2023, 6, 3513−3524

of the phenyl and amine groups result in the better wettability of the bisphenol-F system on the BNNT surface.

Nanocomposites produced by the infusion of the EPON 862/EPIKURE W epoxy resin (i.e., the bisphenol-F resin with the aromatic hardener) into the BNNT and MWCNT buckypaper are shown in Figure S4 in the Supporting Information. Table S6 from Supporting Information shows the comparison of the CNT and BNNT nanocomposites manufactured by a simple infusion test. Measurements of sample mass and dimensions shows that, with equivalent conditions, the CNT-epoxy composites are thicker than the BNNT-epoxy composites and have lower nanotube content (21 wt % CNTs vs, 32 wt % BNNTs) and lower density (1.25 g cm^{-3} vs 1.37 g cm^{-3}, respectively), as shown in Table S6. The thickness of the initial buckypaper increased with epoxy addition in the case with CNTs, while it was unchanged or decreased slightly in the same case for BNNTs (Figure S4). The differences are attributed to the more favorable wetting of BNNTs in comparison to CNTs, which is consistent with the lower contact angles measured on BNNT buckypaper surfaces and with the MD simulations, where BNNT surfaces show better wettability than CNT surfaces. This demonstrates the effect of wettability on the processibility of polymer composites and the synthesis of high-performance composite materials.

6. CONCLUSIONS

The results of this study demonstrate several important points. First, the nanoscale modeling method and force field utilized herein are validated and match the trends observed in related macroscale experiments. Second, the wettability of epoxy is greater on BNNT surfaces than on CNT surfaces for a wide range of temperatures. The interaction between functional groups in the epoxy system with the surface and the local atomic charges at the surface and droplet interface drive the wettability. Third, the wettability of bisphenol-A resins is generally greater than that of bisphenol-F resins on BNNT and CNT surfaces. Finally, aromatic curing agents generally contribute to better wettability relative to aliphatic curing agents, except at higher temperatures when mixed with the bisphenol-A resin. These same conclusions cannot necessarily be drawn for other epoxy/hardener monomer combinations containing arbitrary numbers of functional groups, mixing ratios, and chain lengths. Separate simulations need to be conducted for these other epoxy/hardener systems.

Overall, these observations indicate that BNNTs show better composite manufacturing processibility than CNTs. Because better processability can lead to composites with fewer defects and voids, it is expected that BNNT/epoxy composites can have better strength and durability properties than CNT/epoxy composites under similar processing conditions. Therefore, BNNT-reinforced PMCs are expected to perform better in applications such as aerospace and aeronautical vehicles.

It is important to note that this research is only focused on uncross-linked epoxy systems. Future studies are planned to study the interfacial interactions of the cross-linked systems. Further MD model validation will be possible by comparing predicted mechanical properties to experimentally measured properties.

ASSOCIATED CONTENT

Supporting Information

The Supporting Information is available free of charge at https://pubs.acs.org/doi/10.1021/acsanm.2c05285.

Simulation files including LAMMPS data files for the surface model, droplet model, and contact simulation model; LAMMPS scripts; IFFR parameter set; and BN surface file in .car and .mdf formats (PDF)

Contact angle simulation files; droplet formation simulation files; and IFFR files (ZIP)

AUTHOR INFORMATION

Corresponding Author

Gregory M. Odegard − *Michigan Technological University, Houghton, Michigan 49931, United States;* orcid.org/0000-0001-7577-6565; Email: gmodegar@mtu.edu

Authors

Swapnil S. Bamane − *Michigan Technological University, Houghton, Michigan 49931, United States;* orcid.org/0000-0002-7537-1901

Michael B. Jakubinek − *National Research Council Canada, Ottawa, Ontario K1A 0R6, Canada*

Krishan Kanhaiya − *University of Colorado Boulder, Boulder, Colorado 80309, United States;* orcid.org/0000-0002-3622-2655

Behnam Ashrafi − *National Research Council Canada, Ottawa, Ontario K1A 0R6, Canada*

Hendrik Heinz − *University of Colorado Boulder, Boulder, Colorado 80309, United States;* orcid.org/0000-0002-6776-7404

Complete contact information is available at: https://pubs.acs.org/10.1021/acsanm.2c05285

Notes

The authors declare no competing financial interest.

ACKNOWLEDGMENTS

SUPERIOR, a high-performance computing cluster at Michigan Technological University, was used in obtaining the MD simulation results presented in this publication. The authors would like to thank Michigan Technological University for support this research. Authors also express their gratitude toward the National Research Council, Canada, for supporting experiments performed in this research.

REFERENCES

(1) Kaiser, A. L.; Chazot, C. A. C.; Acauan, L. H.; Albelo, I. V.; Lee, J.; Gair, J. L.; Hart, A. J.; Stein, I. Y.; Wardle, B. L. High-Volume-Fraction Textured Carbon Nanotube-Bis(maleimide) and −Epoxy Matrix Polymer Nanocomposites: Implications for High-Performance Structural Composites. *ACS Appl. Nano Mater.* **2022**, *5*, 9008−9023.

(2) Deshpande, P. P.; Radue, M. S.; Gaikwad, P.; Bamane, S.; Patil, S. U.; Pisani, W. A.; Odegard, G. M. Prediction of the Interfacial Properties of High-Performance Polymers and Flattened CNT-Reinforced Composites Using Molecular Dynamics. *Langmuir* **2021**, *37*, 11526−11534.

(3) Al Mahmud, H.; Radue, M. S.; Chinkanjanarot, S.; Odegard, G. M. Multiscale Modeling of Epoxy-Based Nanocomposites Reinforced with Functionalized and Non-Functionalized Graphene Nanoplatelets. *Polymers* **2021**, *13*, 1958.

(4) Jakubinek, M. B.; Ashrafi, B.; Martinez-Rubi, Y.; Guan, J.; Rahmat, M.; Kim, K. S.; Dénommée, S.; Kingston, C. T.; Simard, B. Boron Nitride Nanotube Composites and Applications. In *Nanotube Superfiber Materials*, 2nd ed; Schulz, M. J., Shanov, V., Yin, Z., Cahay, M., Eds.; William Andrew Publishing, 2019, pp 91−111. DOI: 10.1016/b978-0-12-812667-7.00005-7

(5) Golberg, D.; Bando, Y.; Huang, Y.; Terao, T.; Mitome, M.; Tang, C.; Zhi, C. Boron Nitride Nanotubes and Nanosheets. *ACS Nano* **2010**, *4*, 2979−2993.
(6) Golberg, D.; Bando, Y.; Tang, C. C.; Zhi, C. Y. Boron Nitride Nanotubes. *Adv. Mater.* **2007**, *19*, 2413−2432.
(7) Kim, J. H.; Pham, T. V.; Hwang, J. H.; Kim, C. S.; Kim, M. J. Boron nitride nanotubes: synthesis and applications. *Nano Convergence* **2018**, *5*, 17.
(8) Wang, J.; Ma, F.; Sun, M. Graphene, hexagonal boron nitride, and their heterostructures: properties and applications. *RSC Adv.* **2017**, *7*, 16801−16822.
(9) Falin, A.; Cai, Q.; Santos, E. J. G.; Scullion, D.; Qian, D.; Zhang, R.; Yang, Z.; Huang, S.; Watanabe, K.; Taniguchi, T.; Barnett, M. R.; Chen, Y.; Ruoff, R. S.; Li, L. H. Mechanical properties of atomically thin boron nitride and the role of interlayer interactions. *Nat. Commun.* **2017**, *8*, 15815.
(10) Rasul, M. G.; Kiziltas, A.; Arfaei, B.; Shahbazian-Yassar, R. 2D boron nitride nanosheets for polymer composite materials. *npj 2D Mater. Appl.* **2021**, *5*, 56.
(11) Kausar, A.; Rafique, I.; Muhammad, B. Review of Applications of Polymer/Carbon Nanotubes and Epoxy/CNT Composites. *Polym.-Plast. Technol. Eng.* **2016**, *55*, 1167−1191.
(12) Machado, L. D.; Ozden, S.; Tiwary, C.; Autreto, P. A. S.; Vajtai, R.; Barrera, E. V.; Galvao, D. S.; Ajayan, P. M. The structural and dynamical aspects of boron nitride nanotubes under high velocity impacts. *Phys. Chem. Chem. Phys.* **2016**, *18*, 14776−14781.
(13) Rahmat, M.; Jakubinek, M. B.; Ashrafi, B.; Martinez-Rubi, Y.; Simard, B. Glass Fiber-Epoxy Composites with Boron Nitride Nanotubes for Enhancing Interlaminar Properties in Structures. *ACS Omega* **2022**, *7*, 10674−10686.
(14) Jakubinek, M. B.; Ashrafi, B.; Martinez-Rubi, Y.; Rahmat, M.; Yourdkhani, M.; Kim, K. S.; Laqua, K.; Yousefpour, A.; Simard, B. Nanoreinforced epoxy and adhesive joints incorporating boron nitride nanotubes. *Int. J. Adhes. Adhes.* **2018**, *84*, 194−201.
(15) Sharma, S.; Setia, P.; Chandra, R.; Thakur, N. Experimental and molecular dynamics study of boron nitride nanotube-reinforced polymethyl methacrylate composites. *J. Compos. Mater.* **2019**, *54*, 3−11.
(16) Shin, H.; Yeverovich, E.; Kim, K. S. Poly(4-vinylpyridine) adsorption on boron nitride nanotubes and hexagonal boron nitride: A comparative molecular dynamics study. *J. Mater. Res.* **2022**, *37*, 4483−4495.
(17) Rahmat, M.; Hubert, P. Carbon nanotube-polymer interactions in nanocomposites: A review. *Compos. Sci. Technol.* **2011**, *72*, 72−84.
(18) Goclon, J.; Panczyk, T.; Winkler, K. Investigation of the interfacial properties of polyurethane/carbon nanotube hybrid composites: A molecular dynamics study. *Appl. Surf. Sci.* **2018**, *433*, 213−221.
(19) Hadden, C. M.; Jensen, B. D.; Bandyopadhyay, A.; Odegard, G. M.; Koo, A.; Liang, R. Molecular modeling of EPON-862/graphite composites: Interfacial characteristics for multiple cross-link densities. *Compos. Sci. Technol.* **2013**, *76*, 92−99.
(20) Hadden, C. M.; Klimek-McDonald, D. R.; Pineda, E. J.; King, J. A.; Reichanadter, A. M.; Miskioglu, I.; Gowtham, S.; Odegard, G. M. Mechanical properties of graphene nanoplatelet/carbon fiber/epoxy hybrid composites: Multiscale modeling and experiments. *Carbon* **2015**, *95*, 100−112.
(21) Pisani, W. A.; Radue, M. S.; Patil, S. U.; Odegard, G. M. Interfacial modeling of flattened CNT composites with cyanate ester and PEEK polymers. *Composites, Part B* **2021**, *211*, 108672.
(22) Patil, S. U.; Radue, M. S.; Pisani, W. A.; Deshpande, P.; Xu, H.; Al Mahmud, H.; Dumitrică, T.; Odegard, G. M. Interfacial characteristics between flattened CNT stacks and polyimides: A molecular dynamics study. *Comput. Mater. Sci.* **2020**, *185*, 109970.
(23) Surblys, D.; Yamaguchi, Y.; Kuroda, K.; Kagawa, M.; Nakajima, T.; Fujimura, H. Molecular dynamics analysis on wetting and interfacial properties of water-alcohol mixture droplets on a solid surface. *J. Chem. Phys.* **2014**, *140*, 034505.
(24) Xu, K.; Zhang, J.; Hao, X.; Zhang, C.; Wei, N.; Zhang, C. Wetting Properties of Defective Graphene Oxide: A Molecular Simulation Study. *Molecules* **2018**, *23*, 1439.
(25) Lundgren, M.; Allan, N. L.; Cosgrove, T.; George, N. Wetting of Water and Water/Ethanol Droplets on a Non-Polar Surface: A Molecular Dynamics Study. *Langmuir* **2002**, *18*, 10462−10466.
(26) Sergi, D.; Scocchi, G.; Ortona, A. Molecular dynamics simulations of the contact angle between water droplets and graphite surfaces. *Fluid Phase Equilib.* **2012**, *332*, 173−177.
(27) Ohler, B.; Langel, W. Molecular Dynamics Simulations on the Interface between Titanium Dioxide and Water Droplets: A New Model for the Contact Angle. *J. Phys. Chem. C* **2009**, *113*, 10189−10197.
(28) Grossiord, N.; Miltner, H. E.; Loos, J.; Meuldijk, J.; Van Mele, B.; Koning, C. E. On the Crucial Role of Wetting in the Preparation of Conductive Polystyrene−Carbon Nanotube Composites. *Chem. Mater.* **2007**, *19*, 3787−3792.
(29) Heine, D. R.; Grest, G. S.; Webb, E. B., III Spreading dynamics of polymer nanodroplets. *Phys. Rev. E: Stat., Nonlinear, Soft Matter Phys.* **2003**, *68*, 061603.
(30) Feng, X.; Mo, Y.; Zhao, Y.; Jiang, S. Understanding the temperature and size dependence of the contact angle of Cu/Si(1 1 1): A molecular dynamics study. *Comput. Mater. Sci.* **2018**, *150*, 222−229.
(31) Ye, J.; Zhang, Q.; Li, X.; Wang, X.; Ke, B.; Li, X.; Shen, Z. Effect of the morphology of adsorbed oleate on the wettability of a collophane surface. *Appl. Surf. Sci.* **2018**, *444*, 87−96.
(32) Bamane, S. S.; Gaikwad, P. S.; Radue, M. S.; Gowtham, S.; Odegard, G. M. Wetting Simulations of High-Performance Polymer Resins on Carbon Surfaces as a Function of Temperature Using Molecular Dynamics. *Polymers* **2021**, *13*, 2162.
(33) Heinz, H.; Lin, T.-J.; Kishore Mishra, R.; Emami, F. S. Thermodynamically consistent force fields for the assembly of inorganic, organic, and biological nanostructures: the INTERFACE force field. *Langmuir* **2013**, *29*, 1754−1765.
(34) Winetrout, J. J.; Kanhaiya, K.; Sachdeva, G.; Pandey, R.; Damirchi, B.; van Duin, A.; Odegard, G.; Heinz, H. Implementing Reactivity in Molecular Dynamics Simulations with the Interface Force Field (IFF-R) and Other Harmonic Force Fields. **2021**, arXiv:2107.14418. arXiv preprint.
(35) Gaikwad, P. S.; Krieg, A. S.; Deshpande, P. P.; Patil, S. U.; King, J. A.; Maiaru, M.; Odegard, G. M. Understanding the Origin of the Low Cure Shrinkage of Polybenzoxazine Resin by Computational Simulation. *ACS Appl. Polym. Mater.* **2021**, *3*, 6407−6415.
(36) Sagar Patil, S. S.; Deshpande, P.; Kashmari, K.; Olaya, M.; Odegard, G. Marianna Maiaru In Multi-Scale Approach to Predict Cure-Induced Residual Stresses in an Epoxy System. In *Proceedings of the American Society for Composites—Thirty-fifth Technical Conference*, 2020.
(37) Heinz, H.; Suter, U. W. Atomic Charges for Classical Simulations of Polar Systems. *J. Phys. Chem. B* **2004**, *108*, 18341−18352.
(38) Arash, B.; Wang, Q.; Varadan, V. K. Mechanical properties of carbon nanotube/polymer composites. *Sci. Rep.* **2014**, *4*, 6479.
(39) Thompson, A. P.; Aktulga, H. M.; Berger, R.; Bolintineanu, D. S.; Brown, W. M.; Crozier, P. S.; in 't Veld, P. J.; Kohlmeyer, A.; Moore, S. G.; Nguyen, T. D.; Shan, R.; Stevens, M. J.; Tranchida, J.; Trott, C.; Plimpton, S. J. LAMMPS - a flexible simulation tool for particle-based materials modeling at the atomic, meso, and continuum scales. *Comput. Phys. Commun.* **2022**, *271*, 108171.
(40) Plimpton, S. Fast Parallel Algorithms for Short-Range Molecular Dynamics. *J. Comput. Phys.* **1995**, *117*, 1−19.
(41) Mortazavi, B.; Silani, M.; Podryabinkin, E. V.; Rabczuk, T.; Zhuang, X.; Shapeev, A. V. First-Principles Multiscale Modeling of Mechanical Properties in Graphene/Borophene Heterostructures Empowered by Machine-Learning Interatomic Potentials. *Adv. Mater.* **2021**, *33*, 2102807.

https://doi.org/10.1021/acsanm.2c05285
ACS Appl. Nano Mater. 2023, 6, 3513−3524

(42) Pramanik, C.; Gissinger, J. R.; Kumar, S.; Heinz, H. Carbon nanotube dispersion in solvents and polymer solutions: mechanisms, assembly, and preferences. *ACS Nano* **2017**, *11*, 12805−12816.
(43) Mark, L. O.; Zhu, C.; Medlin, J. W.; Heinz, H. Understanding the Surface Reactivity of Ligand-Protected Metal Nanoparticles for Biomass Upgrading. *ACS Catal.* **2020**, *10*, 5462−5474.
(44) Akkineni, S.; Zhu, C.; Chen, J.; Song, M.; Hoff, S. E.; Bonde, J.; Tao, J.; Heinz, H.; Habelitz, S.; De Yoreo, J. J. Amyloid-like amelogenin nanoribbons template mineralization via a low-energy interface of ion binding sites. *Proc. Natl. Acad. Sci. U.S.A.* **2022**, *119*, No. e2106965119.
(45) Chkhartishvili, L.; Dekanosidze, S.; Maisuradze, N.; Beridze, M.; Esiava, R. Estimation of atomic charges in boron nitrides. *East.-Eur. J. Enterp. Technol.* **2015**, *3*, 50.
(46) Silver, A.; Bray, P. NMR study of bonding in some solid boron compounds. *J. Chem. Phys.* **1960**, *32*, 288−292.
(47) Bray, P. In NMR studies of borates and borides. In *AIP Conference Proceedings*; American Institute of Physics, 1986; pp 142−167.
(48) Damirchi, B.; Radue, M.; Kanhaiya, K.; Heinz, H.; Odegard, G. M.; van Duin, A. C. T. ReaxFF Reactive Force Field Study of Polymerization of a Polymer Matrix in a Carbon Nanotube-Composite System. *J. Phys. Chem. C* **2020**, *124*, 20488−20497.
(49) Evans, D. A. History of the Harvard ChemDraw Project. *Angew. Chem., Int. Ed.* **2014**, *53*, 11140−11145.
(50) Kim, K. S.; Kingston, C. T.; Hrdina, A.; Jakubinek, M. B.; Guan, J.; Plunkett, M.; Simard, B. Hydrogen-Catalyzed, Pilot-Scale Production of Small-Diameter Boron Nitride Nanotubes and Their Macroscopic Assemblies. *ACS Nano* **2014**, *8*, 6211−6220.
(51) Cho, H.; Walker, S.; Plunkett, M.; Ruth, D.; Iannitto, R.; Martinez Rubi, Y.; Kim, K. S.; Homenick, C. M.; Brinkmann, A.; Couillard, M.; Dénommée, S.; Guan, J.; Jakubinek, M. B.; Jakubek, Z. J.; Kingston, C. T.; Simard, B. Scalable Gas-Phase Purification of Boron Nitride Nanotubes by Selective Chlorine Etching. *Chem. Mater.* **2020**, *32*, 3911−3921.

https://doi.org/10.1021/acsanm.2c05285
ACS Appl. Nano Mater. 2023, 6, 3513−3524